中国激光

强光电离氢原子产生花篮状干涉动量谱的数值研究

张晟华[1,2]，张贵忠[1,2*]，付国跃[1,2]，史伟[1,2]，姚建铨[1,2]

[1]天津大学精密仪器与光电子工程学院，天津 300072；

[2]教育部光电信息技术重点实验室，天津 300072

摘要 报道了强激光脉冲电离氢原子诱导的花篮状动量谱(PMDs)的数值模拟研究。采用强场近似理论(SFA)和鞍点近似算法模拟计算了不同激光强度条件下的花篮状动量谱。数值模拟结果表明，花篮状干涉结构电子动量谱源于三种干涉条纹的相互干涉叠加，这三种干涉条纹分别是半圆状阈上电离(ATI)干涉条纹和两种左右对称的周期内干涉(ICI)条纹。后者的干涉条纹随着激光强度的增加而单调变密。依据经典作用相位，深入研究了阈上电离干涉结构和周期内干涉结构的特点，提出了定量描述这两类干涉条纹结构的解析式，所提解析式可以很好地刻画干涉条纹的性质。此外，类比于传统坐标空间的多缝干涉，本文给出了动量空间三缝干涉诱导花篮状动量谱的直观物理图像，该图像有助于理解电子波包干涉的微观机理。

关键词 非线性光学；光电子全息；花篮状干涉动量谱；阈上电离；周期内干涉

中图分类号 O437 **文献标志码** A **DOI**: 10.3788/CJL220769

1 引 言

在强激光场作用下[1-3]，原子中的电子电离后沿不同的路径运动。如果沿不同路径运动的两种电子以相同的最终动量到达探测器，就会发生电子干涉，形成光电子动量谱(PMDs)中的干涉结构[4]。这些干涉结构记录了电子的动力学信息和母核的结构信息，是研究原子分子微观状态和强场微观机理的重要工具。电离的电子通常可分为两类：一类直接到达探测器，该类电子可类比于激光全息中的参考光；另一类在交变激光场的作用下返回母核，发生回碰后再到达探测器，该类电子可类比于激光全息中的信号光。

理论上，通过求解含时薛定谔方程(TDSE)可以得到电子动量谱，但求解含时薛定谔方程的方法难以调控强场中电子运动的微观过程，难以获得微观物理图像。鉴于此，人们一般基于半经典理论进行数值模拟计算。2010 年，Yan 等[5]基于半经典的强场近似(SFA)理论计算了强场电离原子诱导的电子动量谱，计算结果与严格求解含时薛定谔方程的结果吻合较好。2014 年，Bian 等[6]通过求解 HeH^{2+} 体系的含时薛定谔方程，得到了蜘蛛型干涉结构的电子动量谱；同时，他们分析了 4 种光电子全息图样，发现回碰电子对光电子全息图样起决定作用。以往研究的较多的是蜘蛛型电子动量谱[6-7]，它主要沿激光偏振方向分布，其信号最强。2012 年，Korneev 等[8]通过实验测量了氩原子阈上电离(ATI)过程形成的干涉结构，对比分析了通过求解含时薛定谔方程以及通过强场近似理论模拟得到的阈上电离干涉结构，并讨论了库仑势的作用。2017 年，Maxwell 等[9]研究了强场近似理论下氢原子的阈上电离干涉条纹与周期内干涉(ICI)条纹所形成的干涉结构，提出了电子地毯型电子动量谱。事实上，电子地毯型电子动量谱[5,8-22]主要分布在与激光偏振垂直的方向上，其信号强度相对较弱。该类干涉结构也被称作电子扇子状结构[5-7,9,14-15]、电子涡旋状结构[15,17]和花篮状结构[5,9,15-17,21-22]。虽然该类干涉结构的强度较弱，但其携带了阈上电离和周期内干涉的微观过程的特征信息。本团队利用氢原子的强场近似理论和鞍点近似理论，对花篮状电子动量谱的形成过程进行数值研究，得到了一组表达式，该表达式可定量刻画花篮状电子动量谱干涉图样的性质。此外，本研究给出了一种动量空间三缝干涉的物理图像，有助于更好地理解该干涉结构。

2 理论计算方法

在长度规范和偶极近似条件下，激光场中的原子的哈密顿量为

$$H=\frac{\boldsymbol{p}^2}{2}+V(\boldsymbol{r})+\boldsymbol{r}\cdot\boldsymbol{E}(t), \tag{1}$$

式中：$\boldsymbol{E}(t)$为激光电场；$\boldsymbol{p}$为电子动量；$V(\boldsymbol{r})$为原子库仑势；$\boldsymbol{r}$为电子与母核的距离，$\boldsymbol{r}$的方向为母核指向电子。

收稿日期：2022-04-18；**修回日期**：2022-05-18；**录用日期**：2022-06-22；**网络首发日期**：2022-07-06

基金项目：国家自然科学基金(11674243，11674242)、中央高校基本科研基金(3122016D014)

通信作者：*johngzhang@tju.edu.cn

无激光场的哈密顿量的束缚本征态为

$$\psi_i(t)=\psi_i\exp(\mathrm{i}I_p t),\tag{2}$$

式中：ψ_i表示$t=0$时刻的束缚本征态；I_p表示原子的电离能。

在激光场的最强时段，电子被电离。在强场近似理论中，电离的电子被视为自由电子，忽略母核的影响，只计及激光电场的作用，并将电子在激光场中的最终态取为Volkov态。Volkov态[23-26]在长度规范下表示为

$$\left|\varphi_p(t)\right\rangle=\left|\boldsymbol{p}+\boldsymbol{A}(t)\right\rangle\exp\left[-\mathrm{i}S_p(t)\right],\tag{3}$$

其中，

$$S_p(t)=\int_0^t\frac{\left[\boldsymbol{p}+\boldsymbol{A}(t')\right]^2}{2}\mathrm{d}t',\tag{4}$$

$$\left|\boldsymbol{p}+\boldsymbol{A}(t)\right\rangle=\frac{1}{(2\pi)^{\frac{3}{2}}}\exp\left\{\mathrm{i}\left[\boldsymbol{p}+\boldsymbol{A}(t)\right]\cdot\boldsymbol{r}\right\},\tag{5}$$

$\boldsymbol{A}(t)$为激光电场的矢势，$\boldsymbol{A}(t)=-\int_t\boldsymbol{E}(t')\mathrm{d}t'$。Volkov态对应的演化算符为

$$U_p(t,t')=\int\mathrm{d}^3\boldsymbol{k}\left|\varphi_p(t)\right\rangle\left\langle\varphi_p(t')\right|,\tag{6}$$

式中：$\boldsymbol{k}$为电子的正则动量。

在原子单位制下（atomic units，a. u.），电子质量$m=1$，所以末态动量对应的速度表示为$\boldsymbol{v}(t)=\boldsymbol{p}_{\mathrm{constant}}+\boldsymbol{A}(t)$，其中$\boldsymbol{p}_{\mathrm{constant}}$为电子电离时刻的动量。在强场近似理论中，电子的电离振幅[23-27]为

$$M_{pi}^{\mathrm{SFA}}(T_p)=-\mathrm{i}\int_0^{T_p}\mathrm{d}\tau\left\langle\varphi_p(\tau)\left|U_p(T_p,\tau)V_{\mathrm{L}}(\tau)\right|\psi_i(\tau)\right\rangle,\tag{7}$$

式中：T_p为激光脉冲的持续时间；$V_{\mathrm{L}}(\tau)=\boldsymbol{r}\cdot\boldsymbol{E}(\tau)$。总演化算子为

$$U(t,t')=U_p(t,t')-\mathrm{i}\int_{t'}^{t}U(t,\tau)V(\boldsymbol{r})U_p(\tau,t')\mathrm{d}\tau,\tag{8}$$

式中：$U(t,\tau)$为演化算子。由此推导得出电离振幅的零级和一级近似的表达式[23-26]为

$$M_{pi}(T_p)=M_{pi}^{(0)}(T_p)+M_{pi}^{(1)}(T_p)+\cdots,\tag{9}$$

其中，

$$M_{pi}^{(0)}(T_p)=-\mathrm{i}\int_0^{T_p}\left\langle\varphi_p(T_p)\left|U_p(T_p,\tau)V_{\mathrm{L}}(\tau)\right|\psi_i(\tau)\right\rangle\mathrm{d}\tau,\tag{10}$$

$$M_{pi}^{(1)}(T_p)=(-\mathrm{i})^2\int_0^{T_p}\mathrm{d}\tau\left\langle\varphi_p(T_p)\left|\int_\tau^{T_p}\mathrm{d}\tau'U(T_p,\tau')V(\boldsymbol{r})U_p(\tau',\tau)V_{\mathrm{L}}(\tau)\right|\psi_i(\tau)\right\rangle。\tag{11}$$

零级近似对应直接电离过程，而一级近似则对应电子的回碰过程。

在强场近似理论中，一般采用鞍点近似算法进行具体计算。在鞍点近似算法中，需要计算电子的电离时刻t_i和回碰时刻t_r。对于直接电离，其鞍点方程[27-30]为

$$\left.\frac{\partial S_p(t)}{\partial t}\right|_{t=t_s}=\frac{\left[\boldsymbol{p}+\boldsymbol{A}(t_s)\right]^2}{2}+I_p=0。\tag{12}$$

由于I_p为实数，故电离时刻t_s为复数（下标s代表鞍点）。

电离时刻和回碰时刻满足的鞍点方程[31-33]为

$$\begin{cases}\dfrac{\left[\boldsymbol{p}+\boldsymbol{A}(t_i)\right]^2}{2}+I_p=0\\ \left[\boldsymbol{k}+\boldsymbol{A}(t_r)\right]^2=\left[\boldsymbol{p}+\boldsymbol{A}(t_r)\right]^2\\ (t_r-t_i)\boldsymbol{k}=-\displaystyle\int_{t_i}^{t_r}\mathrm{d}t'\boldsymbol{A}(t')\end{cases}。\tag{13}$$

由式(13)可知，只要给定光电子的最终动量$\boldsymbol{p}$，就可以由鞍点方程求解出电子的电离时刻t_i、回碰时刻t_r和动量$\boldsymbol{k}$。对所有鞍点求和得到概率振幅为

$$M(\boldsymbol{p})\propto-\mathrm{i}\sum_s\left\{\det\left[\frac{\partial\boldsymbol{p}_s(T_p)}{\partial\boldsymbol{r}_s(t_s)}\right]\right\}^{-\frac{1}{2}}C(t_s)\exp\left[\mathrm{i}S(\boldsymbol{p},\boldsymbol{r}_s,T_p,t_s)\right],\tag{14}$$

其中，

$$C(t_s)=\sqrt{\frac{2\pi\mathrm{i}}{\partial^2S(\boldsymbol{p},\boldsymbol{r}_s,T_p,t_s)/\partial t_s^2}}\left\langle\boldsymbol{p}+\boldsymbol{A}(t_s)\left|\boldsymbol{E}(t_s)\right|\psi_0\right\rangle,\tag{15}$$

式中：$\boldsymbol{p}_s(T_p)$为在鞍点时的电子动量；$\boldsymbol{r}_s(t_s)$为在鞍点时电子与母核的距离，其方向为母核指向电子；$S(\boldsymbol{p},\boldsymbol{r}_s,T_p,t_s)$为半经典动作相位；$\psi_0$为电子的束缚态。由式(14)计算概率振幅的模平方就可以得到花篮状干涉结构的电子动量谱。

在数值模拟计算中，取线偏振激光脉冲的电场为

$$\boldsymbol{E}(t)=\boldsymbol{E}_0\left(\sin\frac{\omega t}{2N_c}\right)^2\sin(\omega t),\tag{16}$$

式中：ω为激光载波频率；$\left(\sin\dfrac{\omega t}{2N_c}\right)^2$为激光脉冲包络；$N_c$为激光脉冲包含的载波周期数。激光沿$x$轴线偏振，波长为800 nm，对应的频率$\omega=0.058$ a. u.，光强范围为$3.5\times10^{13}\sim7\times10^{15}$ W/cm^2。

3　结果与讨论

如图 1 所示，本团队采用强场近似理论和鞍点近似理论，对不同强度（$I=3.5\times10^{13}\sim7\times10^{15}$ W/cm^2）的激光电离氢原子产生的花篮状电子动量谱进行了数值模拟。虽然图 1(a)～(f)中 6 幅图的干涉条纹随着光强增大而不断变密，但仍有规律可循。如图 1(a)示，整个花篮状干涉结构由三种干涉条纹组成，其中的红虚线表示阈上电离过程诱导的半圆环结构，是由时间上相差一个光学周期的电离电子波包间干涉引起的。图 1(g)中的第一电离时区（第一个红色区域）与第三电离时区之间（第二个红色区域）或者第二电离时区（第一个蓝色区域）与第四电离时区（第二个蓝色区域）之间的电子波包干涉即可产生阈上电离半圆环。图 1(a)中绿色和蓝色实线表示的干涉条纹关于 $p_x=0$ 的动量轴对称分布，是由时间上相差半个光学周期的电离电子波包间干涉引起的。图 1(g)中第一电离时区与第二电离时区之间或者第二电离时区与第三电离时区之间的电子波包干涉属于周期内干涉过程，会诱导周期内干涉圆弧。这些电离过程产生的电子波包之间互相干涉，最终就出现了如图 1(a)～(f)所示的复杂图样，阈上电离和周期内干涉之间的干涉使得这些互相交叉的圆弧变成了一个个互相分离的岛状分布。

接下来详细分析阈上电离干涉条纹和周期内干涉条纹的性质。事实上，实验测量已经证实了阈上电离和周期内干涉结构形成的微观机理。例如，Korneev 等[8]于 2012 年采用 800 nm 波长激光电离氙原子，测量到了电子花篮状电子动量谱。当强激光电离原子时，若激光脉冲的宽度只包含一个载波周期，强光电离过程只存在周期内干涉机理；若激光脉冲的宽度包含两个或两个以上载波周期，强光电离过程中除了存在周期内干涉机理外，还存在阈上电离机理。阈上电离条纹就是电子波包的周期间干涉导致的。

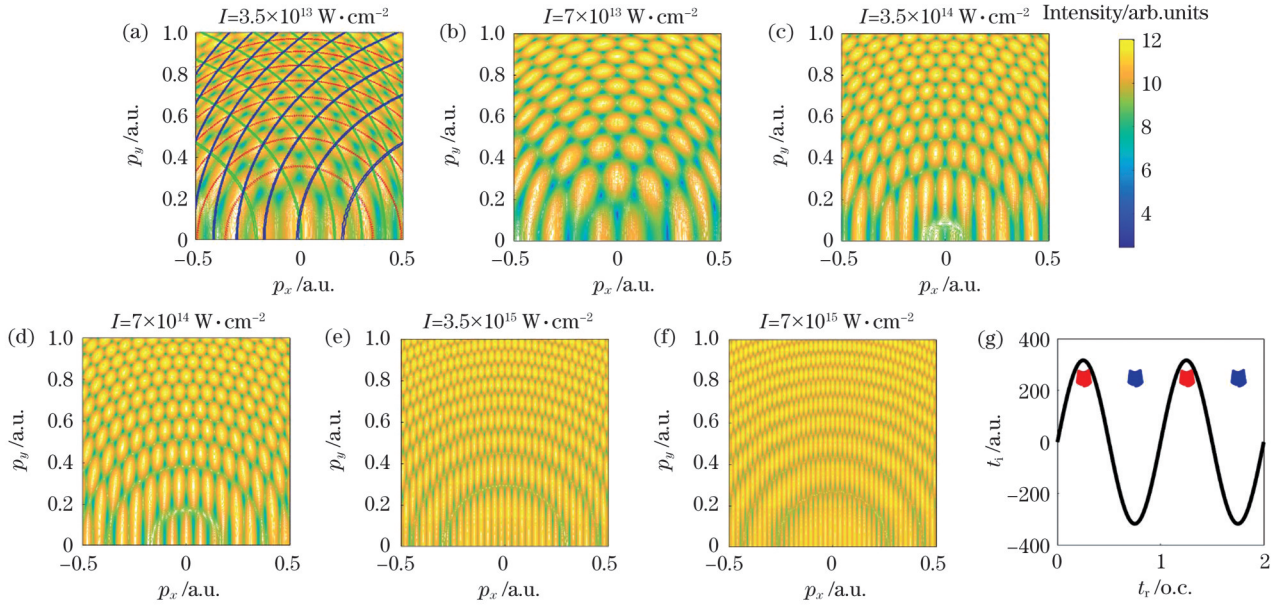

图 1　强激光电离氢原子产生的花篮状干涉结构的电子动量谱以及鞍点区（红色和蓝色区域）和激光电场（黑色实线）。(a)～(f)电子动量谱；(g)4 个鞍点区和激光电场（o. c. 表示激光脉冲载波周期）

Fig. 1　Bouquet-like photoelectron momentum distributions induced by intense laser ionization of hydrogen atom. (a)-(f) Photoelectron momentum distributions; (g) four saddle point zones and laser field (o. c. presents optical cycle)

阈上电离过程产生的干涉条纹是以动量坐标原点为圆心的一系列不等距的半圆环，而且干涉条纹密度随光强变化不明显。图 2(a)给出光强 $I=3.5\times10^{13}$ W/cm^2 时模拟的阈上电离干涉结构，可见：干涉条纹为同心半圆环，圆心在(0,0)处；随着 p_y 增大，条纹单调变密。将其从动量空间变换到能量空间，可以得到图 2(b)。由图 2(b)可以看出，阈上电离干涉条纹为一条条等间隔的水平条纹，条纹间距就是单光子能量。

当光强较小时，原子电离以多光子阈上电离过程为主。阈上电离是一种强场现象，原子会吸收多于电离所必需的光子数，除克服电离能 I_p 和有质动能 U_p 外，吸收的多余光子即产生阈上电离半圆环结构。此光强（$I=3.5\times10^{13}$ W/cm^2）条件下，有质动能为 0.074 a. u.，电离能为 0.5 a. u.，故最小光子数为 $(0.074+0.5)/\omega=10$。即，从第 11 个光子开始对应阈上电离结构，多余光子数 $n_1=11-10=1$。图 2(a)中的干涉条纹可描述为

$$\frac{p_x^2+p_y^2}{2}+\alpha=n_1\omega(n_1=1,2,\cdots),\tag{17}$$

式中：α 为常数，其数值较小，可近似为零；n_1 是吸收的多余光子数，取正整数。式(17)可定量描述阈上电离半圆环干涉结构。图 2(a)中的红色曲线对应 $n_1=1$，是

最靠近动量原点处的一个半圆环。取 $n_1=2$，就可绘制出第二个阈上电离半圆环，以此类推。

形成阈上电离干涉条纹的两类电子所受到的激光电场的作用相同[图 1(g)中的红色电离时区]，只是电离时间相差一个激光载波周期，电子运动对光强的依赖性不明显。实际上，当光强增大到图 1 中的其他数值时，式(17)仍可以描述阈上电离干涉条纹。例如，当光强增大到 $I=7.0\times10^{15}\ \mathrm{W/cm^2}$ 时，模拟的阈上电离干涉结构如图 2(c)所示。此时，Keldysh 参数 $\gamma=0.13$，所以电离过程以隧道电离为主。虽然电离机理还有待深入研究，但可同样根据式(17)绘制出阈上电离干涉结构：取 $n_1=1$，动量分布曲线也是最靠近动量坐标原点的同心半圆环，与数值模拟得到的阈上电离干涉结构吻合较好；取 $n_2=2$，可绘制出第二个阈上电离半圆环，以此类推。图 2(d)是图 2(c)中阈上电离干

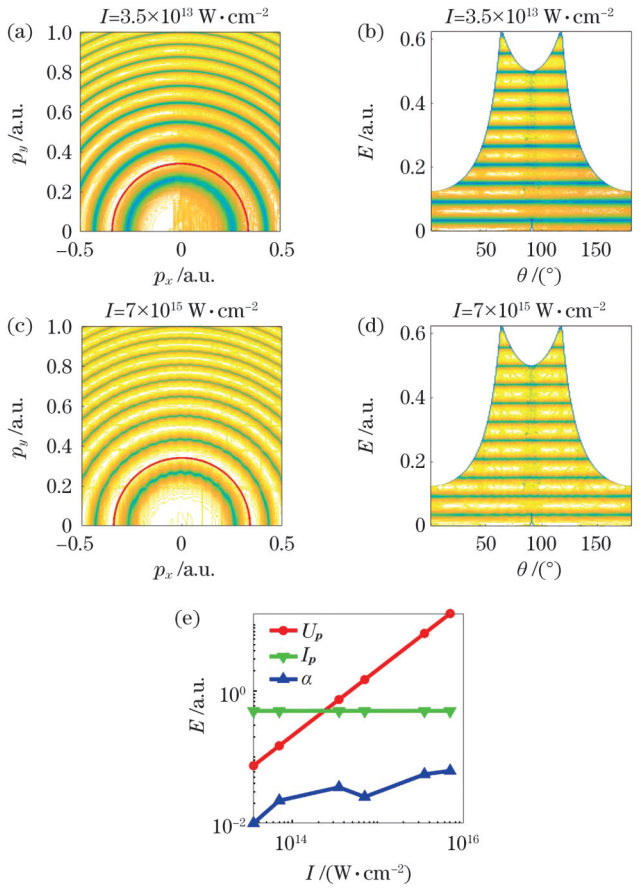

图 2 动量坐标和能量坐标下阈上电离干涉结构以及电子有质动能、电离能和 α 随光强的变化。(a)(c)动量坐标下的半圆环状阈上电离干涉结构；(b)(d)变换到能量坐标下的阈上电离干涉结构；(e)电子有质动能、电离能和 α 随光强的变化

Fig. 2 Above-threshold-ionization fringes in momentum space and energy space and ponderomotive energy, ionization energy and α versus laser intensity. (a)(c) Semi-circle-shaped above-threshold ionization fringes in momentum space; (b)(d) above-threshold ionization fringes in energy space; (e) ponderomotive energy, ionization energy and α versus laser intensity

涉条纹在能量域的图像，相邻条纹之间的能量差也是单光子能量。图 2(e)给出电离能 I_p、有质动能 U_p 和 α 随光强的变化趋势，可见：随着光强不断增加，电子的有质动能单调增加，而电离能为原子的固有属性，不随光强改变，α 的变化较小。

下面分析周期内干涉结构。如果只有周期内干涉过程，那么干涉结构为两组对称的圆弧簇。图 3(a)和图 3(b)给出了两种光强($3.5\times10^{13}\ \mathrm{W/cm^2}$ 和 $7\times10^{15}\ \mathrm{W/cm^2}$)下的模拟计算结果(与动量 $p_x=0$ 呈轴对称分布的另一组未画出)。由图 3(a)、(b)可见，周期内干涉条纹为圆弧段，而且是同圆心。与阈上电离干涉条纹不同，周期内干涉条纹的圆心不在动量坐标原点，而是位于动量 p_x 轴上的其他位置。周期内干涉条纹源于第一电离时区和第二电离时区之间的电子干涉，条纹圆心位于 p_x 正半轴，而第二电离时区和第三电离时区之间的干涉条纹的同心圆的圆心则位于 p_x 负半轴。图 3(a)、(b)表明，随着光强增强，周期内干涉条纹明显单调变密。周期内干涉条纹来源于两类直接电离电子之间的相位差，即

$$\Delta S=\int_{t_1}^{t_2}\frac{1}{2}\left[p_x+\left|\boldsymbol{A}(t)\right|\right]^2\mathrm{d}t+\int_{t_1}^{t_2}\frac{1}{2}p_y^2\mathrm{d}t+\int_{t_1}^{t_2}I_p\,\mathrm{d}t。\tag{18}$$

当该相位差为 2π 的整数(n_2)倍时出现干涉极大。电子动量值(p_x，p_y)满足的方程可由式(18)推导整理为

$$\frac{\left(p_x\pm p_{0x}\right)^2}{2}+\frac{p_y^2}{2}=P_0^2(n_2),\tag{19}$$

其中，

$$p_{0x}=\frac{\beta}{t_\mathrm{r}-t_\mathrm{i}},\tag{20}$$

$$P_0^2(n_2)=\frac{n_2\pi}{t_\mathrm{r}-t_\mathrm{i}}-I_p-\frac{\gamma}{t_\mathrm{r}-t_\mathrm{i}}+\frac{\beta^2}{\left(t_\mathrm{r}-t_\mathrm{i}\right)^2},\tag{21}$$

$$\beta=\frac{A_0}{\omega}(\sin\omega t_\mathrm{r}-\sin\omega t_\mathrm{i}),\tag{22}$$

$$\gamma=\frac{A_0^2}{4}(t_\mathrm{r}-t_\mathrm{i})+\frac{A_0^2}{8\omega}(\sin2\omega t_\mathrm{r}-\sin2\omega t_\mathrm{i}),\tag{23}$$

式中：A_0 是与式(16)对应的激光电场矢势的振幅。(19)式中的正负号表示两套同心圆的圆心对称分布在动量轴 p_x 的两侧，圆心位置是 p_{0x}，圆的半径是 P_0。图 3(a)中的红色曲线是 $n_2=4$ 时由式(19)绘制的曲线，其与数值模拟结果相吻合。$n_2=5$ 对应红色曲线左端的另一干涉圆弧段，以此类推，一直到 $n_2=12$ 为止。类似地，图 3(b)中的红色曲线是 $n_2=130$ 时由式(19)绘制的曲线，其也与数值模拟结果相吻合。整个动量范围对应的 $n_2=117\sim154$。图 3(c)给出的是 p_{0x} 随激光强度的变化。与阈上电离干涉条纹不同，形成周期内干涉条纹的两类电子所受激光电场作用相反[图 1(g)中的红色电离时区和蓝色电离时区]，光强越强，这两类电子的运动差异越大，所以周期内干涉条纹对光强的依赖性越明显。

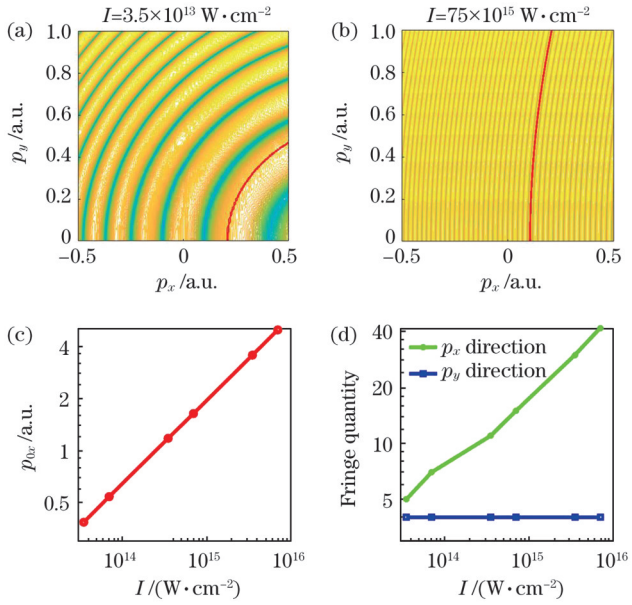

图 3　周期内干涉结构图以及周期内干涉同心圆弧的圆心位置 p_{0x} 和 p_x、p_y 方向上周期内干涉条纹数目随激光强度的变化。(a)(b)圆弧状周期内干涉结构；(c)周期内干涉同心圆弧的圆心位置 p_{0x} 随激光强度的变化；(d) p_x 和 p_y 方向上周期内干涉条纹数目随激光强度的变化

Fig. 3　Inner-cycle interference fringes as well as arc-center positions p_{0x} and interference fringe quantity along p_x and p_y directions versus laser intensity. (a)(b) Arc-shaped inner-cycle interference fringes; (c) inner-cycle interference arc-center positions p_{0x} versus laser intensity; (d) interference fringe quantity along p_x and p_y directions versus laser intensity

图 3(a)和图 3(b)相差较大。为了定量刻画这类周期内干涉结构，沿图 3(a)和图 3(b)的中线(p_x=0 和 p_y=0.5)作纵向和横向切割，计算切割线跨越的干涉条纹数目。计算结果如图 3(d)所示，即 p_x 方向和 p_y 方向上周期内干涉条纹数目随光强的变化。明显可见，随着激光光强增加，p_x 方向上的干涉条纹数目大致呈指数增加，而 p_y 方向上的干涉条纹数目基本不变，有一定的规律可循。

在传统的光学双缝干涉实验中，双狭缝被视作两个光源，其所发出的光波在屏幕处的干涉极大位置构成干涉条纹。上述描述阈上电离和周期内干涉条纹的公式表明，干涉条纹是直角坐标系中的一系列同心圆。受双缝干涉实验的启发，本团队提出了一种动量空间的三缝干涉类比模型，即：由中间狭缝发出的电子波的波前为一组同心半圆环，相邻波前的间隔为激光光子能量，类比于阈上电离半圆环；从左边和右边狭缝发出的电子波的波前也构成一组同心圆弧，相邻波前的间隔也为激光光子能量，类比于周期内干涉圆弧段。这些半圆环和圆弧段的交点就类比于电子花篮状电子动量谱中的干涉极大点，如图 4 所示。图 4(a)中的红色曲线代表上述阈上电离半圆环，而绿色和蓝色曲线代表两组周期内干涉圆弧段，这三类曲线的交点[图 4(a)中的黄色点和图 4(b)中的点]就构成干涉极大分布图。该类比模型有助于更好地理解电子花篮状电子动量谱的形成过程。

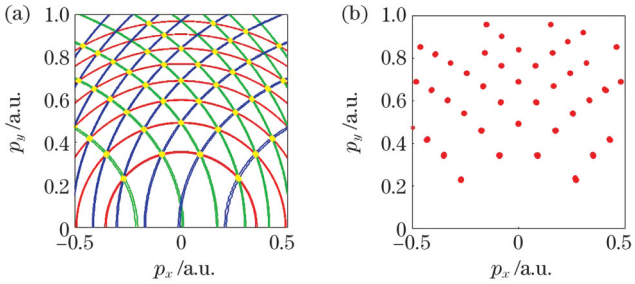

图 4　电子花篮状电子动量谱的三缝干涉模型和电子花篮状电子动量谱中的干涉极大位置。(a)电子花篮状电子动量谱的三缝干涉模型，其中红绿蓝三色曲线代表三组电子波的波前，黄色交点为干涉极大位置；(b)电子花篮状电子动量谱中的干涉极大位置

Fig. 4　Triple slit model for bouquet-like photoelectron momentum distributions and interferometric maxima in electron bouquet-like photoelectron momentum distributions. (a) Triple slit model for bouquet-like photoelectron momentum distributions, where the red, green and blue curves represent the wavefront of three groups of electron waves, and the yellow intersection is the position of interferometric maxima; (b) interferometric maxima in electron bouquet-like photoelectron momentum distributions

4　结　　论

采用强场近似理论和鞍点近似算法对强激光电离氢原子诱导的花篮状干涉结构的光电子动量谱进行了数值模拟研究。结果表明，花篮状干涉结构可分解为阈上电离过程产生的半圆环干涉条纹和周期内干涉过程产生的对称圆弧段干涉条纹。通过经典相位分析总结出了两个定量描述上述两类干涉结构的解析公式。此外，本文给出了动量空间三缝干涉物理图像，该图像可重现花篮状电子动量谱，为研究电子波包干涉提供了一种新思路。

参　考　文　献

[1]　付星，刘廷昊，雷新星，等. 二极管泵浦重复频率纳秒高能固体激光器研究进展[J]. 中国激光，2021，48(15)：1501003.
Fu X，Liu T H，Lei X X，et al. High energy diode-pumped reprated nanosecond solid-state laser[J]. Chinese Journal of Lasers，2021，48(15)：1501003.

[2]　宁永强，陈泳屹，张俊，等. 大功率半导体激光器发展及相关技术概述[J]. 光学学报，2021，41(1)：0114001.
Ning Y Q，Chen Y Y，Zhang J，et al. Brief review of development and techniques for high power semiconductor lasers[J]. Acta Optica Sinica，2021，41(1)：0114001.

[3]　刘运全，韩猛. 强激光场原子隧道电离的研究新进展[J]. 光学学报，2021，41(1)：0102001.
Liu Y Q，Han M. Recent research advances in strong-field atomic tunneling ionization[J]. Acta Optica Sinica，2021，41(1)：0102001.

[4] 唐久, 张贵忠, 何宇飞, 等. 从氢原子的蜘蛛状动量谱提取散射振幅相位[J]. 光学学报, 2021, 41(10): 1002001.
Tang J, Zhang G Z, He Y F, et al. Scattering-amplitude phase extraction from spiderlike photoelectron momentum distributions of hydrogen atoms[J]. Acta Optica Sinica, 2021, 41(10): 1002001.
[5] Yan T M, Popruzhenko S V, Vrakking M J J, et al. Low-energy structures in strong field ionization revealed by quantum orbits[J]. Physical Review Letters, 2010, 105(25): 253002.
[6] Bian X B, Bandrauk A D. Orientation-dependent forward-backward photoelectron holography from asymmetric molecules[J]. Physical Review A, 2014, 89(3): 033423.
[7] Murakami M, Zhang G P. Observation of attosecond electron dynamics in the photoelectron momentum distribution of atoms using few-cycle laser pulses[J]. Physical Review A, 2020, 101(5): 053439.
[8] Korneev P A, Popruzhenko S V, Goreslavski S P, et al. Interference carpets in above-threshold ionization: from the Coulomb-free to the Coulomb-dominated regime[J]. Physical Review Letters, 2012, 108(22): 223601.
[9] Maxwell A S, Al-Jawahiry A, Das T, et al. Coulomb-corrected quantum interference in above-threshold ionization: working towards multitrajectory electron holography[J]. Physical Review A, 2017, 96(2): 023420.
[10] Liu H, Liu Y Q, Fu L B, et al. Low yield of near-zero-momentum electrons and partial atomic stabilization in strong-field tunneling ionization[J]. Physical Review Letters, 2012, 109(9): 093001.
[11] Arbó D G, Ishikawa K L, Persson E, et al. Doubly differential diffraction at a time grating in above-threshold ionization: intracycle and intercycle interferences[J]. Nuclear Instruments and Methods in Physics Research Section B: Beam Interactions with Materials and Atoms, 2012, 279: 24-30.
[12] Li M, Geng J W, Liu H, et al. Classical-quantum correspondence for above-threshold ionization[J]. Physical Review Letters, 2014, 112(11): 113002.
[13] Xie H, Li M, Li Y, et al. Intra-half-cycle interference of low-energy photoelectron in strong midinfrared laser fields[J]. Optics Express, 2016, 24(24): 27726-27737.
[14] Shvetsov-Shilovski N I, Lein M, Madsen L B, et al. Semiclassical two-step model for strong-field ionization[J]. Physical Review A, 2016, 94(1): 013415.
[15] Maxwell A S, Popruzhenko S V, de Morisson Faria C F. Treating branch cuts in quantum trajectory models for photoelectron holography[J]. Physical Review A, 2018, 98(6): 063423.
[16] Shvetsov-Shilovski N I, Lein M, Madsen L B. Multielectron polarization effects in strong-field ionization: narrowing of momentum distributions and imprints in interference structures[J]. Physical Review A, 2018, 98(2): 023406.
[17] Maxwell A S, de Morisson Faria C F, Lai X Y, et al. Spiral-like holographic structures: unwinding interference carpets of Coulomb-distorted orbits in strong-field ionization[J]. Physical Review A, 2020, 102(3): 033111.
[18] Fetić B, Becker W, Milošević D B. Extracting photoelectron spectra from the time-dependent wave function: comparison of the projection onto continuum states and window-operator methods[J]. Physical Review A, 2020, 102(2): 023101.
[19] Tan J, Zhou Y M, Xu S L, et al. Analyzing the electron trajectories in strong-field tunneling ionization with the phase-of-the-phase spectroscopy[J]. Optics Express, 2021, 29(23): 37927-37944.
[20] Murakami M, Chu S I. Photoelectron momentum distributions of the hydrogen atom driven by multicycle elliptically polarized laser pulses[J]. Physical Review A, 2016, 93(2): 023425.
[21] Han M, Ge P P, Shao Y, et al. Revealing the sub-barrier phase using a spatiotemporal interferometer with orthogonal two-color laser fields of comparable intensity[J]. Physical Review Letters, 2017, 119(7): 073201.
[22] Chen J H, Zhao S F, Han M, et al. Photoelectron momentum distributions of F^- ions by a few-cycle laser pulse[J]. Optics Express, 2018, 26(11): 14086-14096.
[23] Keldysh L V. Ionization in the field of a strong electromagnetic wave[J]. Soviet Physics JETP, 1965, 20(5): 1307-1314.
[24] Faisal F H M. Multiple absorption of laser photons by atoms[J]. Journal of Physics B: Atomic and Molecular Physics, 1973, 6(4): L89-L92.
[25] Reiss H R. Effect of an intense electromagnetic field on a weakly bound system[J]. Physical Review A, 1980, 22(5): 1786-1813.
[26] Faisal F H M. Collision of electrons with laser photons in a background potential[J]. Journal of Physics B: Atomic and Molecular Physics, 1973, 6(11): L312-L315.
[27] Gribakin G F, Kuchiev M Y. Multiphoton detachment of electrons from negative ions[J]. Physical Review A, 1997, 55(5): 3760-3771.
[28] Madsen L B, Nikolopoulos L A A, Kjeldsen T K, et al. Extracting continuum information from $\Psi(t)$ in time-dependent wave-packet calculations[J]. Physical Review A, 2007, 76(6): 063407.
[29] Guo L, Chen S, Liu M Q, et al. Rescattering time-energy analysis of high-order above-threshold ionization in few-cycle laser fields[J]. Physical Review A, 2020, 101(3): 033415.
[30] Dubois J, Chandre C, Uzer T. Envelope-driven recollisions triggered by an elliptically polarized pulse[J]. Physical Review Letters, 2020, 124(25): 253203.
[31] Frolov M V, Manakov N L, Minina A A, et al. Control of harmonic generation by the time delay between two-color, bicircular few-cycle mid-IR laser pulses[J]. Physical Review Letters, 2018, 120(26): 263203.
[32] Luo S Q, Li M, Xie W H, et al. Exit momentum and instantaneous ionization rate of nonadiabatic tunneling ionization in elliptically polarized laser fields[J]. Physical Review A, 2019, 99(5): 053422.
[33] Li M, Liu M M, Geng J W, et al. Experimental verification of the nonadiabatic effect in strong-field ionization with elliptical polarization[J]. Physical Review A, 2017, 95(5): 053425.

Numerical Investigation of Bouquet-Like Photoelectron Momentum Distributions in Strong Field Ionization of Hydrogen

Zhang Shenghua[1,2], Zhang Guizhong[1,2*], Fu Guoyue[1,2], Shi Wei[1,2], Yao Jianquan[1,2]

[1]*College of Precision Instrument and Optoelectronics Engineering, Tianjin University, Tianjin* 300072, *China*;
[2]*Key Lab of Optoelectronic Information Technology, Ministry of Education, Tianjin* 300072, *China*

Abstract

Objective In a stronger laser field, electrons move along different paths after ionization. This process involves two phases: first, the electron moves directly to the detector, and second, the ion scatters the other. Interference occurs when the electrons arrive at the

detector with the same final momenta. Moreover, an interference structure in the photoelectron momentum distributions (PMDs) appeared. The interference structure encodes the dynamic information of electrons and the structural information of the parent ions, which are vital tools for studying the microscopic states of atoms and molecules in strong-field processes. Generally, these two kinds of ionized electrons are named reference electron: reaching the detector directly and being analogous to the reference light in laser holography, and the signal electron: returning to the parent ion and being scattered off by the ion and reaching the detector eventually, being analogous to the signal light in laser holography.

Theoretically, we can obtain the PMDs by solving the time-dependent Schrödinger equation (TDSE); however, solving TDSE is difficult because of the microscopic process control to achieve the best nanoscopic physical picture. Therefore, the semiclassical theory becomes an alternative in numerical simulation. The distributed bouquet-like PMDs in momentum domains perpendicular to the laser polarization is relatively weak. However, this interference structure carries the characteristic information of the above-threshold ionization (ATI) and the inner-cycle interference (ICI) processes.

Methods The study used the strong field approximation (SFA) theory and saddle point approximation method for investigations. Electrons are ionized at the peak of the laser field. In SFA, ionized electrons are affected only by the laser field, whereas the influence of parent ions is negligible. The final state of the ionized electron in the laser field was considered the Volkov state. It is simple to obtain the PMDs from the expression of the wave function amplitude of ionized electrons. We used the saddle point approximation method to calculate the bouquet-like PMDs. Moreover, we obtained the ionization time and rescattering time of the electrons and calculated the probability amplitudes by summing all the saddle points to obtain PMDs. Similarly, we carefully examined the bouquet-like PMDs produced by hydrogen atom ionization concerning laser intensity variations in the numerical investigation.

Results and Discussions We used the SFA and the saddle point approximation theory to simulate the bouquet-like PMDs of hydrogen atom ionization under different laser intensities. The light intensity range was $3.5\times10^{13}-7\times10^{15}$ W/cm^2, as shown in Fig. 1. The overall bouquet-shaped interference structure consists of various interference fringes: the ATI process-induced semicircle structure and the ICI process-induced partial circle structure. The interference of the electron wave packets generated by these two ionization processes results in the formation of bouquet-like PMDs. The coherent superposition between the ATI and ICI processes further turns these intersected circles into isolated island-shaped patterns.

The ATI interference fringes are concentric semicircles with centers at $p_x=0$ and $p_y=0$. As the perpendicular momentum p_y increases, these fringes become highly monotonically denser in the PMDs. When the PMDs are converted from the momentum space to the energy space, the ATI interference fringes become horizontal with equal spacing. This spacing is equivalent to the single photon energy (Fig. 2). We derive a formula for the quantitative description of the ATI interference fringes valid over the laser intensity range of 3.5×10^{13}–7×10^{15} W/cm^2.

Although the ICI interference fringes are also partial circles, these interference fringes center at the symmetric positions on the parallel momentum p_x axis. The ICI interference fringes are generated from the electrons ionized at the laser peak and valley times within the same optical cycle. The centers of the ICI interference fringes are located symmetrically in the positive and negative parts of the parallel momentum axis p_x. When the light intensity increases, the ICI interference fringes become highly denser. We also obtained a formula to describe the properties of the ICI interference fringes.

Additionally, we proposed an analog model of triple-slit interference in momentum space to better understand the formation of the bouquet-like PMDs. The wavefronts of electron waves that emanate from the middle slit form a set of concentric semicircles. These represent the ATI semicircles. The wavefronts of electron waves that ensue from the left and right slits form two symmetric concentric partial circles, representing the ICI partial circles. The intersections of these semicircles and partial circles are analogous to the interference maxima in the electronic bouquet-like PMDs (Fig. 4). Similarly, this intuitive model can help understand other interference processes in the strong field ionization of atoms and molecules.

Conclusions We performed an extensive numerical simulation of the bouquet-like PMDs induced by the stronger laser ionization of hydrogen atoms using SFA and saddle point approximation theories. The results show that the bouquet-like interference structure can be decomposed into semicircle-shaped interference fringes generated using the ATI process and partial-circle-shaped interference fringes obtained using the ICI process. We derived two analytical formulas using the classical action phase analysis to describe these two types of interference structures. These are valid over a relatively large laser intensity range. Furthermore, we proposed a physical picture of triple-slit interference in momentum space, which could help understand the bouquet-like PMDs, shedding light on studying electronic interference in strong field processes.

Key words nonlinear optics; photoelectron holography; bouquet-like photoelectron momentum distributions; above-threshold ionization; inner-cycle interference